International Transaction Journal of Engineering, Management, & Applied Sciences & Technologies

http://www.TuEngr.com, http://go.to/Research

A Land Data Assimilation System Utilizing Low Frequency Passive Microwave Remote Sensing: A Case Study of the Tibetan Plateau

David Kuria[a*], Toshio Koike [b], Moses Gachari [a], and Souhail Boussetta [b, c]

[a] *Department of Geomatic Engineering and Geospatial Information Science, Kimathi University College of Technology, KENYA*
[b] *River and Environmental Engineering Laboratory, Department of Civil Engineering, Faculty of Engineering, The University of Tokyo, JAPAN*
[c] *Currently at: European Centre for Medium-Range Weather Forecasts, UNITED KINGDOM*

ARTICLEINFO

Article history:
Received 15 March 2011
Received in revised form
2 June 2011
Accepted 3 June 2011
Available online
6 June 2011

Keywords:
Soil moisture retrieval,
Land Surface Modelling,
Data assimilation,
Passive microwaves,
AMSR-E,
Tibetan Plateau,
Surface emission model

ABSTRACT

To address the gap in bridging global and smaller modelling scales, downscaling approaches have been reported as an appropriate solution. Downscaling on its own is not wholly adequate in the quest to produce local phenomena, and in this paper we use a physical downscaling method combined with data assimilation strategies, to obtain physically consistent land surface condition prediction.

Using data assimilation strategies, it has been demonstrated that by minimizing a cost function, a solution utilizing imperfect models and observation data including observation errors is feasible. We demonstrate that by assimilating lower frequency passive microwave brightness temperature data using a validated theoretical radiative transfer model, we can obtain very good predictions that agree well with observed conditions.

1. Introduction

While General Circulation Models (GCMs) are best at simulating evolving and future changes in climate systems, they are unable to produce mesoscale and local atmospheric

*Corresponding author (David Kuria). Tel: +254-727-399208. E-mail addresses: dn.kuria@gmail.com. ©2011. International Transaction Journal of Engineering, Management, & Applied Sciences & Technologies. Volume 2 No.3. ISSN 2228-9860. eISSN 1906-9642. Online Available at http://TuEngr.com/V02/303-324.pdf

phenomena (Wilks, 1999). Thus downscaling methods are necessary to bridge the gap between global scales and other smaller modelling scales. In this paper we use a high resolution mesoscale model and nest it within a GCM. This nesting is realized by using initial and boundary conditions from GCM output. This approach alone is not adequate for reproducing local phenomena and extreme events because nesting does not include accurate land surface initial and boundary conditions, missing important physical processes such as convection and local circulation (Boussetta, 2005).

Many satellite based microwave imaging systems have been launched in space. Some of the recent ones include the Scanning Multichannel Microwave Radiometer (SMMR) launched in 1978 and Special Sensor Microwave Imager (SSM/I) launched in 1987. More recent sensors launched include Advanced Microwave Scanning Radiometer on board Earth Observing Satellite (AMSRE) and Tropical Rainfall Monitoring Mission (TRMM). These systems provide observations of variables that describe the earth's atmosphere, ocean, cryosphere and land surface (Njoku, 1999). To aid in the interpretation of imagery from such sensors, microwave radiative transfer models have been developed, which are used to express propagation of microwaves in media, such as in Ulaby et al. (1981), Tsang et al. (1985), and Wilheit et al. (1999).

Data assimilation employs models and observations exploiting the strengths of each. Models are approximations of physical processes, and these approximations introduce errors due to varying degrees of inaccuracy in representing these processes. On the other hand, observations while recording actual situations include random observations errors. In addition, due to costs incurred in obtaining these observations, they are more often than not inadequate, and are not uniformly distributed in time and space. Thus, models or observations on their own are not adequate in representing actual physical systems being studied or monitored. By applying data assimilation approaches, these limitations in model representation and in obtaining observations can be offset.

Data assimilation techniques have evolved within meteorology and physical oceanography and in operational numerical weather prediction for atmospheric and oceanic flows (Ide et al., 1997). These concepts have recently been applied to small scales, but this has largely been in attempts to improve estimation of soil moisture by assimilation of microwave TBs (Mahadevan

et al., 2003, 2007; Reichle et al., 2001). In mesoscale modelling, it is critical to provide reliable initial and boundary conditions. GCM forecast and analysis products can provide such data, but these have to be downscaled to the mesoscale before they can be used. By combining downscaling and data assimilation techniques, better initial conditions can be obtained, which can thereafter be used to run the mesoscale model, giving better forecasts. Sensitivity of L-X microwave bands to surface conditions has been exploited in the past in retrieving soil moisture conditions (Njoku, 1999). Since at these frequencies the atmosphere can be assumed transparent, clarification of surface emission heterogeneity through field experiment has a potential of supporting a retrieval scheme for land surface conditions.

By exploiting data assimilation approaches and using a physically based surface emission model as observation operator, there is potential to obtain better land surface condition prediction by assimilating lower frequency microwave brightness temperatures. To physically address the mechanisms of land-atmosphere interactions based on land surface conditions, the Land Data Assimilation System developed by Boussetta (2005) is used to augment the stand-alone mesoscale model. While this system addresses land surface heterogeneities, it does not address atmospheric components in a direct way. This is not critical since this research is restricted to using lower frequency brightness temperatures in the data assimilation exercise. This system assimilates lower frequency (6.925 – 18.7 GHz) microwave TBs to improve estimation of land surface conditions. In this paper we build on the work done by Boussetta (2005), by including as observation operator an improved surface emission model that was validated by Kuria et al. (2007).

Data assimilation is a method of estimating a set of parameters by optimizing the fit between the solution and a set of observations which the model is meant to predict (Bannister, 2001). In this context, the procedure of adjusting the model parameters until the model 'best predicts' the observables is referred to as optimization. The observations used for data assimilation can be very heterogeneous with respect to their temporal and spatial resolution, and their type. The results of an assimilation scheme are a continuous data set, which represents the best estimate for the state of the system. This is done by optimizing the state vector of the system using available observations and dynamic constraint of the numerical model, specified by the governing dynamical equations.

*Corresponding author (David Kuria). Tel: +254-727-399208. E-mail addresses: dn.kuria@gmail.com.

In variational data assimilation not only is a a close fit to one observation (the last one) required but additionally, consistency with a dynamic model over a defined period of time (Daley, 1991). This means that in variational data assimilation, one tries to adjust the model globally to fit all observations during the assimilation period.

A discrete model for the evolution of an atmospheric, coupled system from time t_i to time t_{i+1} is governed by the equation

$$x^f(t_{i+1}) = \mathbf{M}[x^f(t_i)] \tag{1}$$

where x and M are the model's state vector and its corresponding dynamics (model) operator, respectively. The state vector x has dimension n. **M** represents the model simulation or prediction, and may differ from equation (1) if the model is nonlinear and/or deterministic. The state vector x describes the state variables.

Observations y^0 at time t_i are defined by

$$y_i^0 = \mathbf{H}_i[x^f(t_i)] + \varepsilon_i \tag{2}$$

where **H** is an observation operator, and ε is noise or observation errors. The observation vector $y_i^0 \equiv y_i^0(t_i)$ has dimension p_i. A major problem of data assimilation is that, typically, $p_i \ll n$. The observation operator **H**, can be nonlinear, like **M**, and both can contain explicit time dependence - denoted by subscript *i* - in addition to the implicit dependence via the state vector $x_i^f \equiv x_i^f(t_i)$. The error ε is assumed to have a normal distribution with mean 0. Its covariance matrix is denoted by **R**, consisting of instrumental and observation errors.

In variational data assimilation one tries to adjust the model's initial parameters x_0, globally to all observations available during the assimilation period. Therefore it is necessary to introduce a scalar quantity **J**, which represents the difference between the model and observed states. The objective function is a function of the state vector x. **J** is the sum of the background error $\mathbf{J}_B$, which gives the difference between the model state and the background x_b and an observation error $\mathbf{J}_0$, which gives the difference between the model state and observations The complete cost function can be written as;

$$\mathbf{J} = \mathbf{J}_B + \mathbf{J}_0 \tag{3}$$

The common form of $\mathbf{J}_B$ is expressed as

$$\mathbf{J}_B(x_0) = \frac{1}{2}(x_0 - x_0^b)^T \mathbf{B}^{-1}(x_0 - x_0^b) \tag{4}$$

where, x_0 is the analysis variable, or state vector, x_0^b is the background field, and **B** is the background error covariance matrix.

The common form of $\mathbf{J}_0$ is given as

$$\mathbf{J}_0(x_0) = \frac{1}{2}\sum_{i=1}^{N}\left((\mathbf{H}_i[x_i] - y_i^0)^T \mathbf{R}_i^{-1}(\mathbf{H}_i[x_i] - y_i^0)\right)$$

$$x_i = \mathbf{M}(t_i, t_0)(x_0) \tag{5}$$

where, y^0 represents all of the satellite observations, **H** is the observation operator, **M** is the model operator, and **R** is the observational error covariance matrix. In this paper, y^0 represents remotely sensed microwave brightness temperatures, and **H** is a radiative transfer model, which computes corresponding brightness temperatures. N is the length of an assimilation window. Thus, relatively accurate observations are used directly to correct model-estimated values, and these corrections are fed back in the solution process.

The total cost function can be rewritten in as follows:

$$\mathbf{J}(x_0) = \frac{1}{2}\sum_{i=1}^{N}\left((\mathbf{H}_i[x_i] - y_i^0)^T \mathbf{R}_i^{-1}(\mathbf{H}_i[x_i] - y_i^0)\right)$$

$$+\frac{1}{2}(x_0 - x_0^b)^T \mathbf{B}^{-1}(x_0 - x_0^b) \tag{6}$$

Various assumptions have been made when formulating the above cost function. The first assumption is that the models are 'perfect' over the assimilation period, which leads to the

*Corresponding author (David Kuria). Tel: +254-727-399208. E-mail addresses: dn.kuria@gmail.com.

so-called strong-constraint formalism. An alternative cost function could be written with a third term, as an additional constraint to penalize model errors. This would be an example of a weak constraint formalism (Mahadevan et al., 2007). Due to its compactness, we adopt this strong-constraint approach in this paper.

2. Meso scale model run

Figure 1 shows the Tibet Coordinated Enhance Observing Period (CEOP) site. The Tibetan plateau is located in Asia with an area of approximately 3000 × 1000 km2 and a mean elevation of more than 4 km above mean sea level.

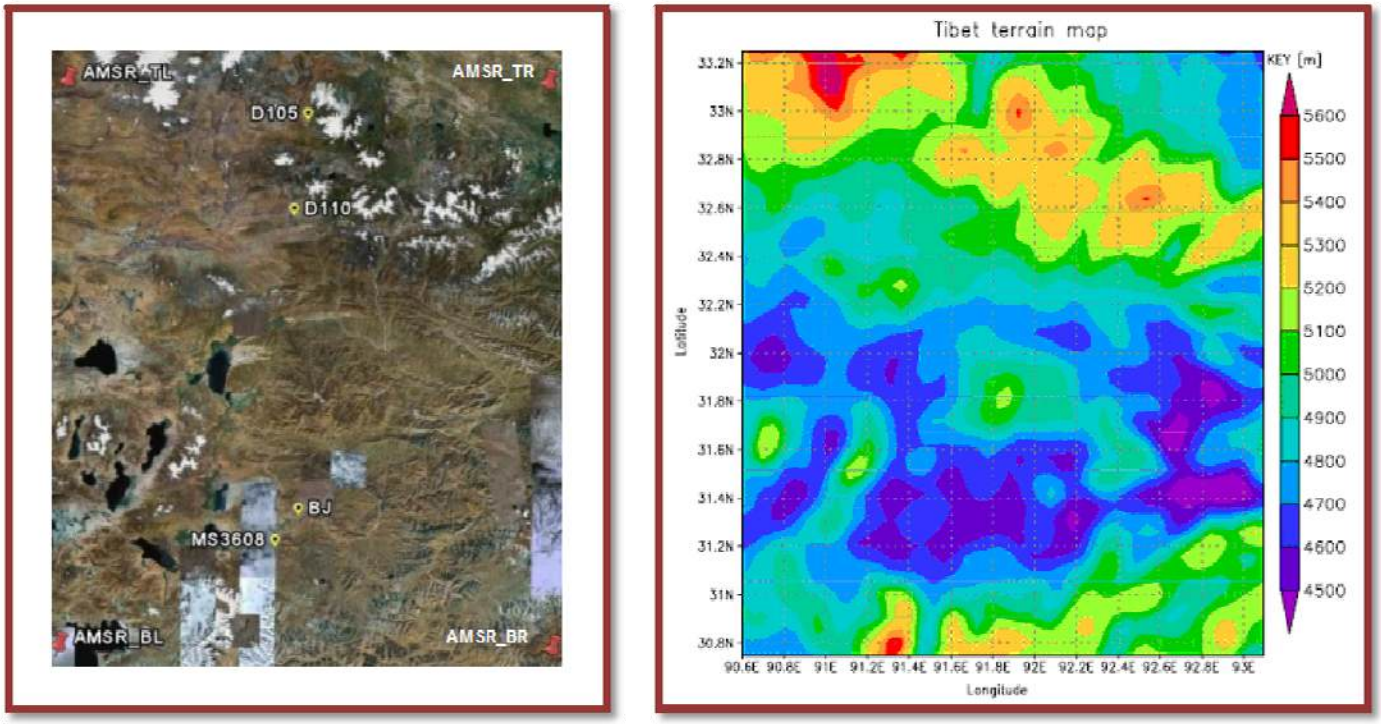

(a) (b)

Figure 1: CEOP Tibet Site: (a) Satellite imagery, with red pegs marking the extents corresponding to AMSR-E image. Marked with small yellow pegs are 4 in-situ stations. This image was obtained from Google Earth. (b) Terrain map generated by ARPS.

It is bounded by the highest mountains in the world (Himalayas, Kunlun shan, Pamir). It is considered an important component of the global water and energy cycle as it exerts appreciable thermal and dynamic influences on the local and regional meteorology as well as on the Northern Hemisphere atmospheric circulations (Yang et al., 2009).

Table 1: Model domain specifications.

Variable	Description	Setting
Δx	East West spacing	5560 m (0.05°)
Δy	North South spacing	5643 m (0.05°)
λ_m	Central longitude	91.9°E
φ_m	Central latitude	32.0°N
n_x	East West grids	70
n_y	North South grids	70
n_z	Vertical levels	41

While there are other mesoscale models such as the Weather Research and Forecasting (WRF) model and the Fifth-Generation Penn State Mesoscale Model (MM5), the Advanced Regional Prediction System (ARPS) developed at the Center for Analysis and Prediction of Storms (CAPS) (Xue et al., 2003) as the mesoscale model for simulating surface and atmospheric evolution of Tibetan Plateau conditions. ARPS was used since a coupling of this model had been done with Simple Biosphere Model (SiB2) and had demonstrated good results in simulating land surface conditions (Boussetta, 2005). Table 1 defines the domain settings of Tibet area used in the simulation and validation exercise. This area is about 390 × 390 km^2 providing ample overlap over an AMSR-E brightness image covering an area of about 280 × 280 km^2 with central position defined as (32°N, 91.9°E). The z- dimension is staggered with higher resolution provided near surface (30 m) and smoothly transitioning to lower resolution at higher elevations (1.2 km). This is to significantly improve simulation of near surface features which vary rapidly over time. The simulation were undertaken to simulate three days evolution of land and atmosphere condition. This period was from 19th August 2004 00:00 UTC – 22nd August 2004 00:00 UTC. The integration time steps were as follows: (i) evolution of surface condition (120 seconds) (ii) small time step (1 second) and (iii) big time step (6 seconds).

2.1 Initial and Boundary conditions

For this paper, we used National Centers for Environmental Prediction (NCEP) Global Forecast System (GFS) reanalysis data to provide initial and boundary conditions for running the Mesoscale model. The GFS is a global spectral data assimilation and forecast system. GFS forecasts are produced every 6 hour. The output product has a horizontal resolution of 1° and

*Corresponding author (David Kuria). Tel: +254-727-399208. E-mail addresses: dn.kuria@gmail.com. International Transaction Journal of Engineering, Management, & Applied Sciences & Technologies. Volume 2 No.3. ISSN 2228-9860. eISSN 1906-9642. Online Available at http://TuEngr.com/V02/303-324.pdf

vertically it has 64 layers with model top layer at 0.2 hPa.

We used the EXT2ARPS package to generate the required lateral boundary forcing, linearly interpolated in time to the domain of our model run. This GFS generated boundary conditions were updated every 6 hours. The package ARPSTRN generated terrain data from 30"× 30" global topographic dataset provided by Center for Analysis and Prediction of Storms (CAPS) University of Oklahoma. Temporal invariant surface condition was interpolated from 30" soil maps, land use maps and 10' Normalized Difference Vegetation Index (NDVI) data using ARPSSFC package.

2.2 Model parameters used

To sufficiently simulate smaller scale atmospheric features related to land surface effect, our domain horizontal resolution was set to 0.05° × 0.05° while for the vertical grid ARPS uses a hyperbolic tangent function to stretch the grid interval in this case from 30 m at the surface to nearly 1.2 km at the top (18 km).

The physics parameterization options include a 1.5-order Turbulent Kinetic Energy-based subgrid scale closure scheme turbulence, and a planetary boundary layer parameterization. Radiative forcing is computed according to an atmospheric radiation transfer parameterization and is updated each 10 minutes.

The Simplified Biosphere (SiB) model, developed by Sellers et al. (1986) and subsequently revised to SiB2 in Sellers et al. (1996), is used as surface scheme, and the Lin Ice Microphysics parameterization (Lin et al., 1983) to parameterize cloud and precipitation. For explicitly resolving convection, the modified Kain-Fritsch convective scheme is better suited for resolving convection (Truong et al, 2009), the original Kain-Fritsch convective parameterization (Kain and Fritsch, 1993) was adopted, since LDAS is mainly sensitive to land surface conditions. The model domain topography is derived from 1 km resolution global dataset.

Land cover was obtained from the global dataset based on the global ecosystem classification with a spatial resolution of 30" × 30" while its associated static parameters were derived according to Sellers et al. (1996). Soil types were obtained from global dataset with a resolution of 30" × 30" and vegetation types were obtained from a 100 resolution global

dataset. All these datasets were obtained from CAPS

3. Land Data Assimilation Scheme

Boussetta (2005) validated Land Data Assimilation Scheme (LDAS) by assimilating satellite data and assessed its dynamic downscaling ability. He applied it in a three dimensional configuration on a mesoscale area of the Tibetan plateau. In his case, he used GEWEX Asian Monsoon Experiment (GAME) Tibet dataset for 1998. This system combines a land data assimilation scheme with a coupled land-atmosphere mesoscale model in a recursive cycle. The system runs by first introducing the initial and boundary atmospheric conditions from NCEP GFS into the coupled land-atmosphere mesoscale model (ARPSSiB2). This coupled model then produces forcing for one assimilation window to the land data assimilation system which optimizes the initial surface variables and feeds them back to the coupled land-atmosphere model (Figure 2).

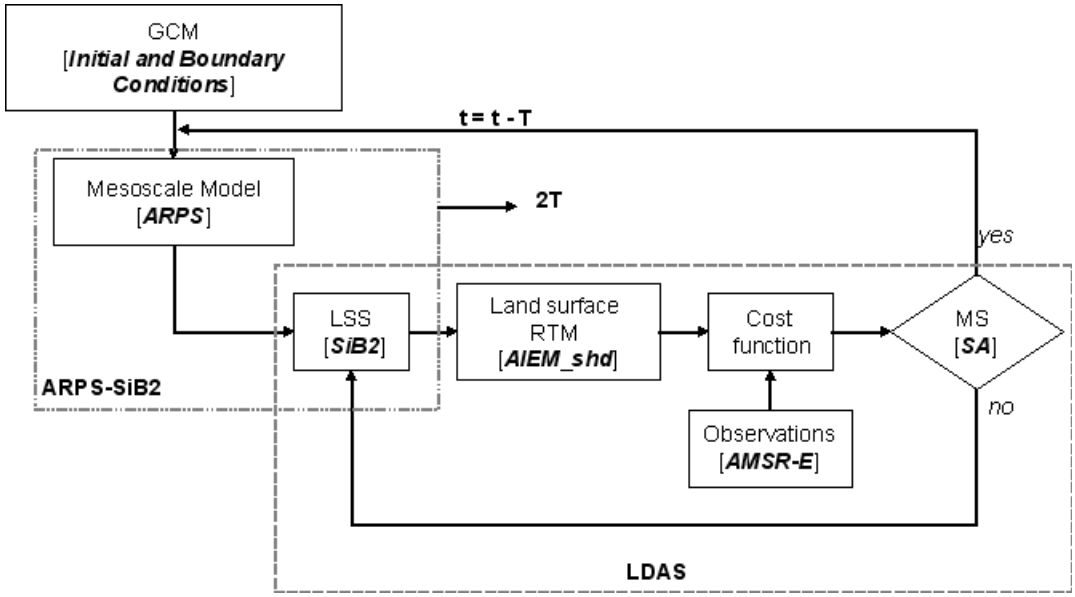

Figure 2: Land Data Assimilation Scheme.

Figure 3 shows LDAS assimilation cycle. A typical LDAS assimilation cycle comprises of the following steps.

Step 1 : ARPS-SiB2 is run for an assimilation window time T to obtain an initial guess and forcing parameters for LDAS.

Step 2 : LDAS runs for one assimilation window, which feeds back new initial surface condition for ARPS-SiB2 at time t = t − T.

*Corresponding author (David Kuria). Tel: +254-727-399208. E-mail addresses: dn.kuria@gmail.com.

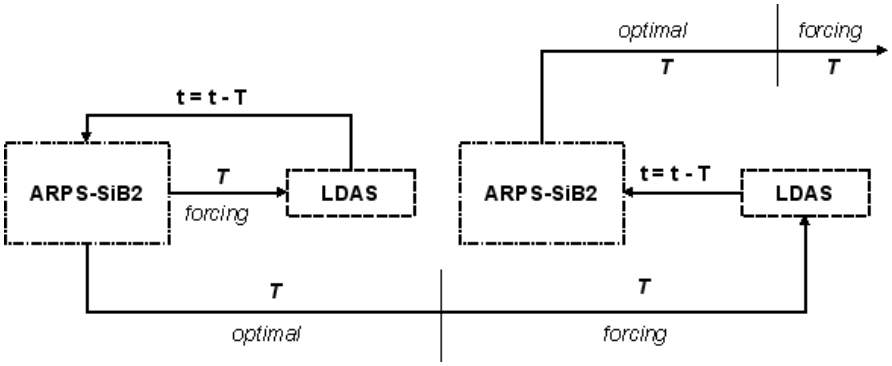

Figure 3: LDAS Assimilation Cycle.

Step 3 : ARPS-SiB2 runs for two assimilation window time 2T, the first window output being considered as optimal, while the second one serves as forcing for the LDAS run.

In this paper, we used a 24 hour assimilation window (T = 24h). This was due to the need to have at least one satellite observation to be assimilated during the assimilation period.

3.1 Model operator

SiB2 is used as the model operator in the assimilation scheme. It is a dual source model with fluxes originating from soil surface and canopy. It incorporates simple representations of vertical soil moisture transport, plant controlled transpiration, interception, evaporation, infiltration, sensible and heat fluxes through physically based mechanisms.

SiB2 includes three soil layers; a surface soil layer of a few centimeters which acts as a significant source of direct evaporation when moist; a root zone which is the supplier of soil moisture to the roots and accounts for transpiration; and a deep soil layer acting as a source for hydrological base flow and upward recharge to the root zone.

3.2 Observation operator

Boussetta (2005) assimilated TRMM Microwave Imager (TMI) satellite brightness temperature (TB) observations at 10.7 and 19.4 GHz, both polarizations. In this paper, we used AMSR-E TB observations at 10.7 and 18.7 GHz both polarizations. Additionally, assimilation of two surrogate observations, namely Polarization Index (PI) proposed by Paloscia and Pampaloni (1988) at 6.9 GHz, and Index of Soil Wetness (ISW) developed by Fujii and Koike

(2001), derived using 18.7 and 6.9 GHz horizontal polarization. These three frequencies' data were chosen due to their relative insensitivity to atmospheric conditions. These two relationships are given as,

$$PI_6 = \frac{TB_{6v} - TB_{6h}}{\frac{1}{2}(TB_{6v} + TB_{6h})} \tag{7}$$

$$ISW = \frac{TB_{18h} - TB_{6h}}{\frac{1}{2}(TB_{18h} + TB_{6h})} \tag{8}$$

where *v* or *h* in the subscript denote polarization i.e vertical and horizontal respectively at the given frequency.

Boussetta (2005) used a first order radiative transfer model (RTM) coupled with QH model of Choudhury et al. (1979) for addressing surface roughness effects. In Kuria et al. (2007) it was shown that the QH model is not fit for use with high frequency data. Although it has been widely used, its roughness parameters have to be 'calibrated' first, and are thus not physically based. While this is sufficient in most cases when dealing with frequencies lower than 20 GHz, the lack of a physical basis in determining these parameters motivated us to consider using the improved surface emission model validated by Kuria et al. (2007). This surface emission model is used as the observation operator. Compared to that used in Boussetta (2005), it uses a physically based treatment of surface roughness effects, thereby improving confidence of forward modelling. A further refinement was by introducing Polarization Index (PI) and Index of Soil Wetness (ISW) that describe roughness and moisture conditions as surrogate observations. We use the variance matrix of the following form to describe the background co-variance matrix **B**, used in equation 4.

$$\mathbf{B} = \begin{bmatrix} \sigma^2_{T_g} & 0 & 0 & 0 & 0 \\ 0 & \sigma^2_{T_d} & 0 & 0 & 0 \\ 0 & 0 & \sigma^2_{Mv_{sfc}} & 0 & 0 \\ 0 & 0 & 0 & \sigma^2_{Mv_{rt}} & 0 \\ 0 & 0 & 0 & 0 & \sigma^2_{Mv_{dp}} \end{bmatrix} \tag{9}$$

The observation error covariance matrix (**R**), used in equation 5, follows a similar form

*Corresponding author (David Kuria). Tel: +254-727-399208. E-mail addresses: dn.kuria@gmail.com. International Transaction Journal of Engineering, Management, & Applied Sciences & Technologies. Volume 2 No.3. ISSN 2228-9860. eISSN 1906-9642. Online Available at http://TuEngr.com/V02/303-324.pdf

$$\mathbf{R} = \begin{bmatrix} \sigma^2_{Tb_{10h}} & 0 & 0 & 0 & 0 & 0 \\ 0 & \sigma^2_{Tb_{10v}} & 0 & 0 & 0 & 0 \\ 0 & 0 & \sigma^2_{Tb_{18h}} & 0 & 0 & 0 \\ 0 & 0 & 0 & \sigma^2_{Tb_{18v}} & 0 & 0 \\ 0 & 0 & 0 & 0 & \sigma^2_{PI_6} & 0 \\ 0 & 0 & 0 & 0 & 0 & \sigma^2_{ISW_{618}} \end{bmatrix} \quad (10)$$

In these cases we assume that all observations are uncorrelated, and model state variables are uncorrelated too. In Table 2, we list values of observation errors, and in Table 3, values of background errors used in the observation and background error matrices, respectively as used in this research. The background covariance matrix was assumed static for simplicity, though ideally it should be allowed to evolve with the assimilation process, being updated with new values for use in subsequent steps.

Table 2: Observation errors

Tb_{10h}	Tb_{10v}	Tb_{18h}	Tb_{18v}	PI_6	ISW_{618}
4K	3K	5K	4K	0.01	0.01

Simulated Annealing was used to minimize the cost function **J**. It is a heuristic optimization approach capable of minimizing the variational cost function without using adjoint models (Ingber, 1993). It avoids problems due to strong non-linearities and discontinuities in finding the global minimum in the hilly structure of the cost function. It is based on the analogous approach of metal annealing in thermodynamics (Kirkpatrick et al., 1983).

Table 3: Background errors

T_g	T_d	Mv_{sfc}	Mv_{rt}	Mv_{dp}
3K	2K	0.04	0.03	0.02

4. Results and discussion

We use ARPS/LDAS to simulate land surface conditions using AMSR-E lower frequency (6.925, 10.65, and 18.7 GHz) brightness temperatures (TBs) for Tibetan plateau. This

simulation was for three days from 00:00 UTC on 19th August 2004 – 00:00 UTC on 22nd August 2004.

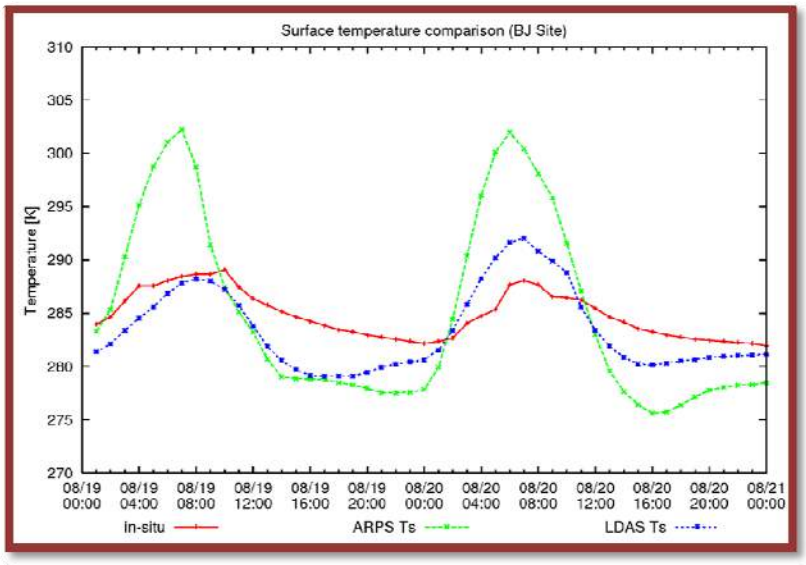

(a)

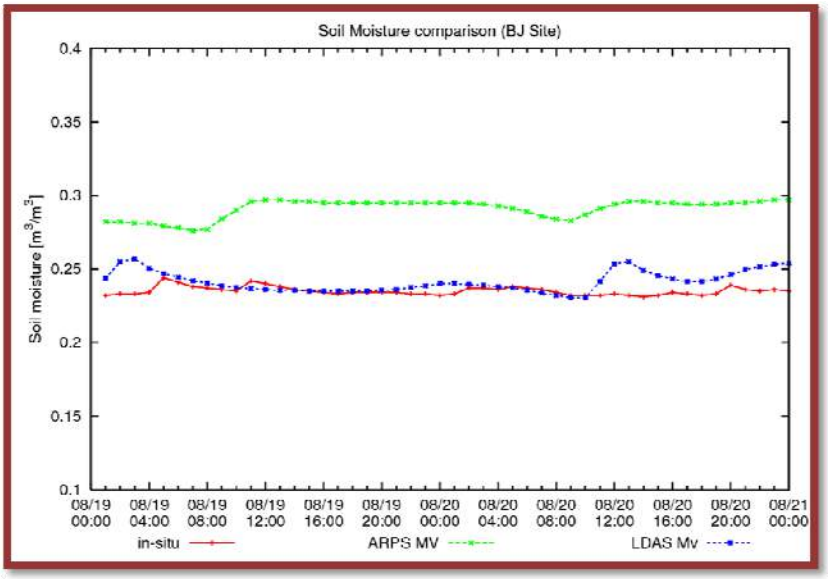

(b)

Figure 4: Comparison of time-series land surface variables (a) surface temperature and (b) surface soil moisture at BJ site

4.1 Time series comparison

We run ARPS/LDAS assimilation as one case, and plain ARPS as second case. Both models were run for 72 hours from 00:00 UTC 19/08/2004 to 00:00 UTC 22/08/2004. In Figure 4 we show comparisons of retrieved surface variables at BJ site.

*Corresponding author (David Kuria). Tel: +254-727-399208. E-mail addresses: dn.kuria@gmail.com. International Transaction Journal of Engineering, Management, & Applied Sciences & Technologies. Volume 2 No.3. ISSN 2228-9860. eISSN 1906-9642. Online Available at http://TuEngr.com/V02/303-324.pdf

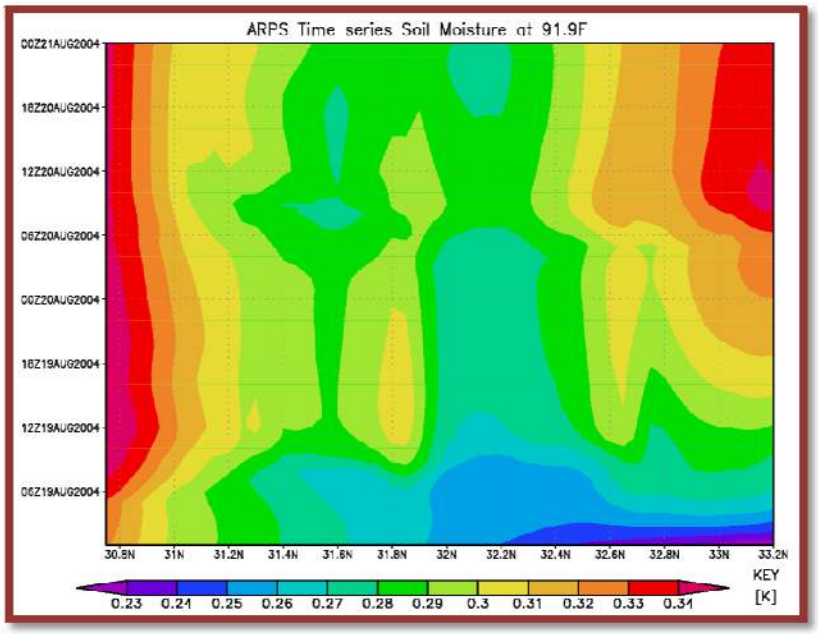

(a)

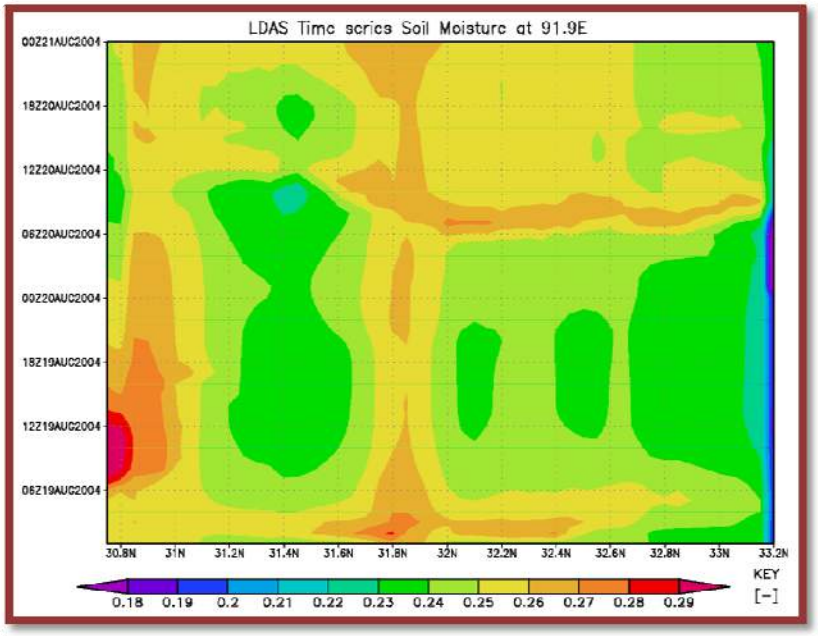

(b)

Figure 5: Time series soil moisture product comparison along 91.9°E (a) ARPS case and (b) LDAS case

We prepared a time series plot covering the duration 0 – 48h, and we compare this with an in-situ dataset. This in-situ data set comprises hourly soil moisture records at 3cm and 10cm depth, and soil temperature at the same depths. Since we are using Microwave observations which sense shallow depths, we will analyze only near surface variables (3cm depth). During

this time period, we have two AMSR-E overpasses, descending overpass at 19:41 UTC on 19th August and ascending overpass 06:42 UTC on 20th August.

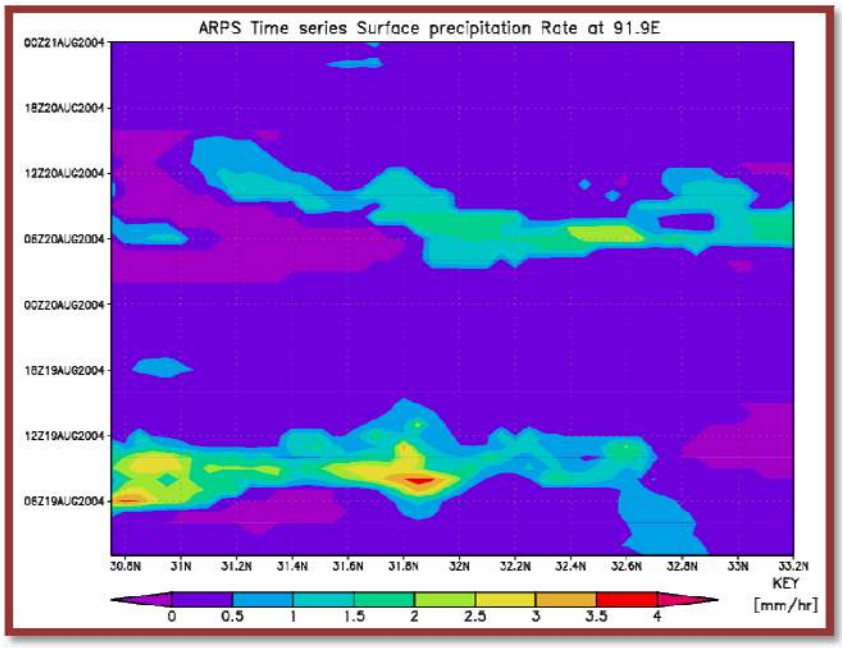

(a)

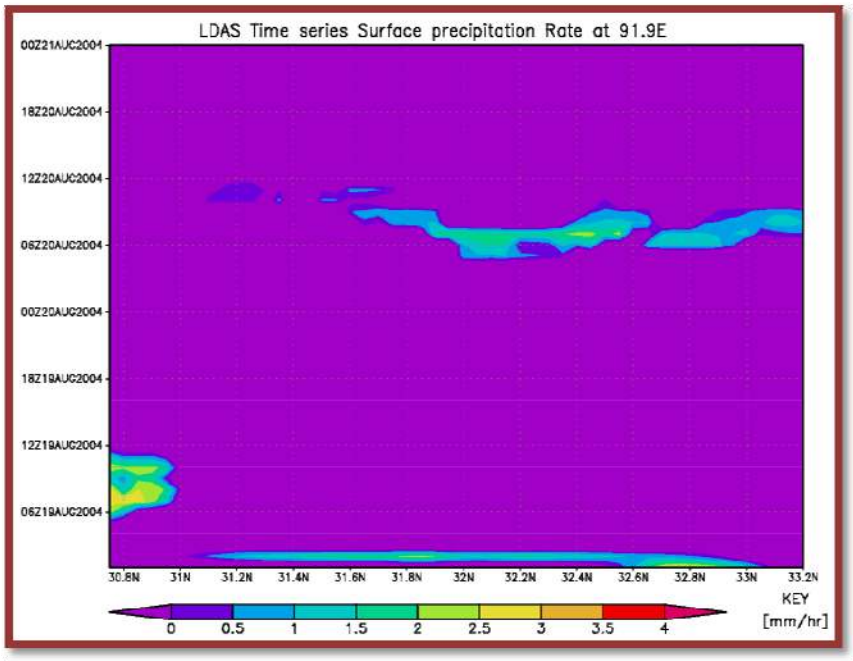

(b)

Figure 6: Time series surface precipitation comparison along 91.9°E (a) ARPS case and (b) LDAS case

*Corresponding author (David Kuria). Tel: +254-727-399208. E-mail addresses: dn.kuria@gmail.com. International Transaction Journal of Engineering, Management, & Applied Sciences & Technologies. Volume 2 No.3. ISSN 2228-9860. eISSN 1906-9642. Online Available at http://TuEngr.com/V02/303-324.pdf

We begin by considering surface temperature (Figure 4(a)).While bearing in mind the fact that we are comparing grid averaged values with point observations, we note that (i) the diurnal variation of near surface temperature observed is simulated by both cases, (ii) ARPS derived surface temperature have much higher peaks and valleys than ARPS/LDAS case and (iii) in general, the ARPS/LDAS configuration gives better agreement with the in-situ dataset, though the gap between peaks/valley can vary by as much as 5 K.

Considering near surface soil moisture (Figure 4(b)), there is remarkable agreement with in-situ dataset for ARPS/LDAS case. ARPS case is over-predicting soil moisture by as much as 5%. At the time slots corresponding to AMSR-E overpass times it can be noted that ARPS/LDAS and in-situ datasets match perfectly, and also that in the interval between these times, the simulations follows observations almost perfectly.

In Figure 5 we show comparison of time series moisture product along longitude 91°E.We take the same period (0 – 48h) for this analysis. It is clear that the ARPS case (Figure 5(a)) is wetter than the corresponding ARPS/LDAS case. We note that ARPS case is wettest at the edges, alluding to the strong influence of initial and boundary conditions from GFS reanalysis data. The situation is different in ARPS/LDAS case. ARPS seems to get wetter implying heavy precipitation events at the beginning (6 hours after start) and about 30 hours after start. We have similar events in ARPS/LDAS but their duration and intensity is not as high as in ARPS case. Figure 6 depicts time series precipitation for the same period. As mentioned above, it can be seen that ARPS is producing higher precipitation, in intensity and distribution. We note too that ARPS precipitating durations are longer than ARPS/LDAS precipitation durations.

4.2 Comparison of simulation at hour closest AMSR-E overpass time

We consider 07:00 UTC on August 20th 2004 for analysis of soil moisture retrieval. Figure 7 shows simulation following the same convention, i.e. ARPS case (Figure 7(a)) and ARPS/LDAS case (Figure 7(b)). Soil moisture distribution in ARPS case is strongly influenced by the initial conditions giving rather high forecasts of soil moisture.

Its soil moisture distribution follows GFS soil moisture distribution (not shown). Soil moisture distribution in ARPS/LDAS case by assimilating observed TBs shows improved distribution.

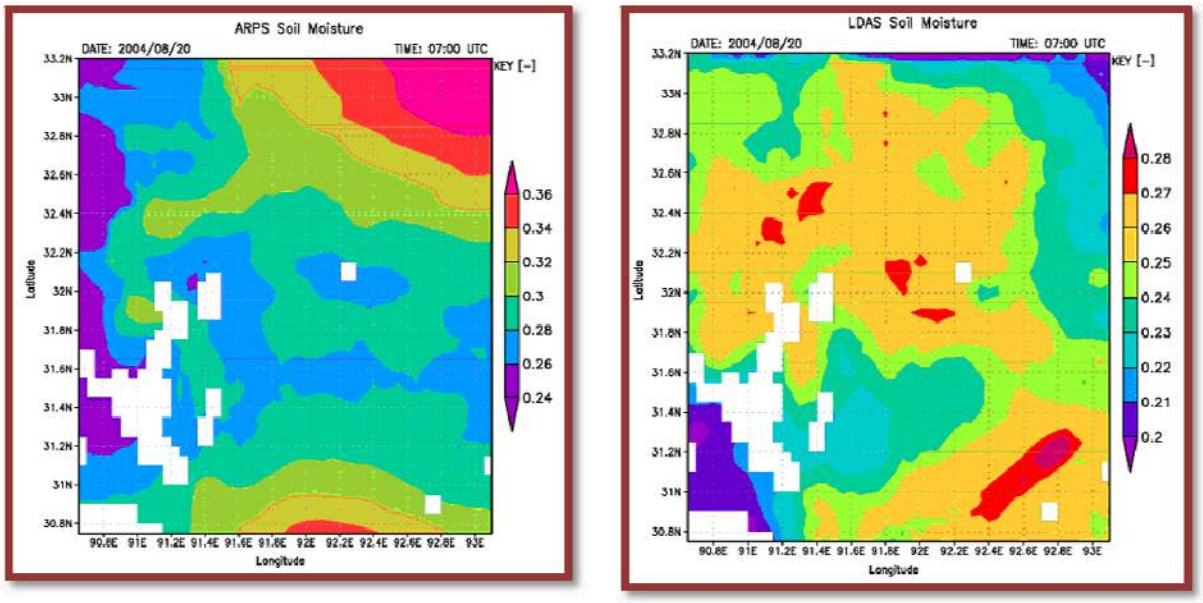

(a) (b)

Figure 7: Moisture comparison (a) ARPS and (b) LDAS for August 20th 2004.

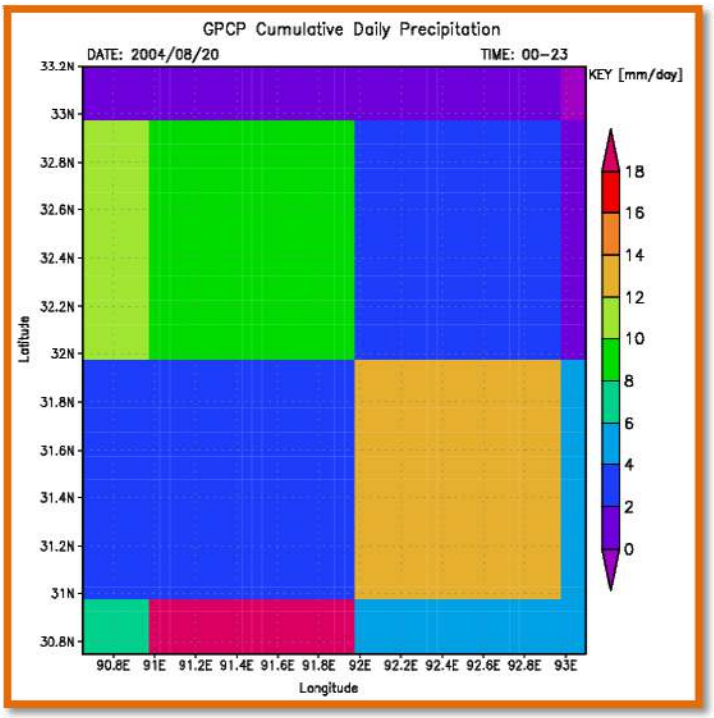

Figure 8: GPCP Cumulative surface precipitation

To validate this hypothesis, we consider the relationship between precipitation and soil moisture. It is known that the occurrence of a precipitation event invariably leads to an increase in soil moisture, thus in the absence of quantitative soil moisture observations or estimates,

*Corresponding author (David Kuria). Tel: +254-727-399208. E-mail addresses: dn.kuria@gmail.com. International Transaction Journal of Engineering, Management, & Applied Sciences & Technologies. Volume 2 No.3. ISSN 2228-9860. eISSN 1906-9642. Online Available at http://TuEngr.com/V02/303-324.pdf

observed precipitation (or precipitation deduced from observations) can be used to give a qualitative assessment of soil moisture.

We include Global Precipitation Climatology Project (GPCP) daily cumulative precipitation data for the site on August 20th, to assist in verifying our hypothesis that ARPS/LDAS case is significantly better than ARPS case. GPCP provides daily global gridded values of cumulative precipitation, for the period from October 1996 – December 2006 (Huffman et al., 2001). The product considered for this validation exercise is the 1° resolution daily precipitation dataset. Figure 8 shows this GPCP dataset for the spatial domain considered in this paper. Comparing this with our simulations, it can be noted that while the resolution of GPCP is very coarse, we have similar pattern with the ARPS/LDAS case. The ARPS case is completely different with the observed precipitation pattern.

Considering surface temperature simulations (Figure 9), surface temperature representation in both cases follows similar patterns, but on closer inspection, it can be noted that ARPS simulated generally higher temperatures than ARPS/LDAS case.

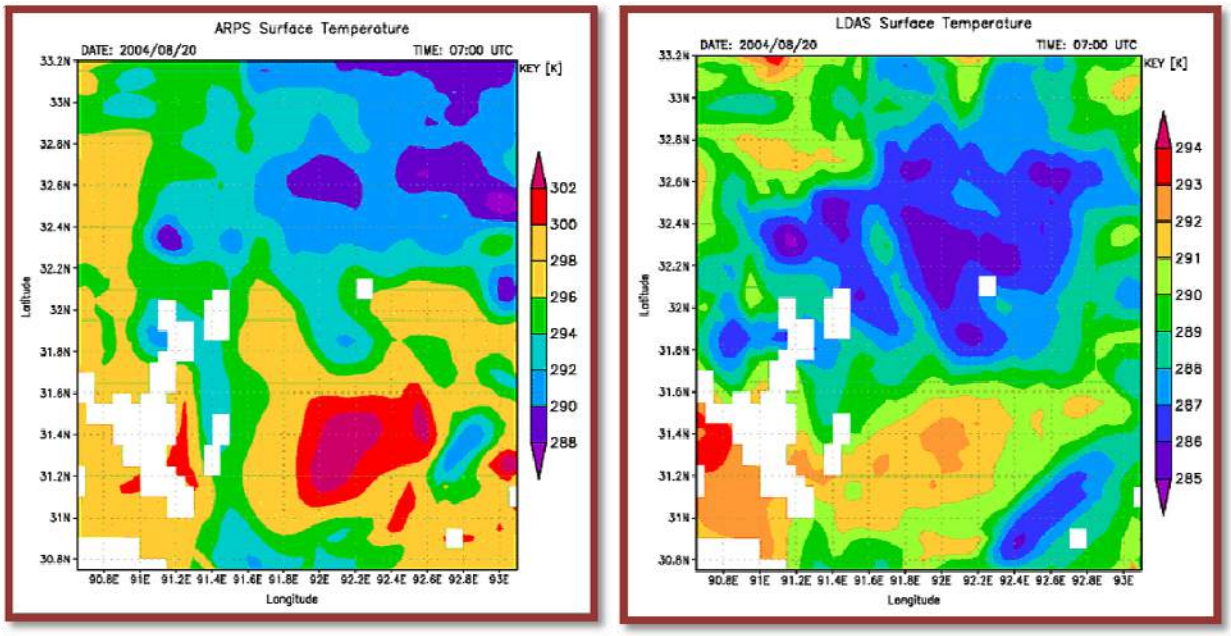

(a) (b)

Figure 9: Surface temperature comparison (a) ARPS and (b) LDAS for August 20th 2004

Additionally, when we compare ARPS/LDAS case with terrain map (Figure 1), we note that the temperature distribution shows agreement with terrain map (high temperature

corresponding to valley area, and low temperatures corresponding to mountain areas).

We also note that in the central region of ARPS/LDAS case we have colder temperatures. This region corresponds could be experiencing a precipitation event at this time (bearing in mind the time series results shown in Figure 6). It can thus be argued that ARPS/LDAS simulated surface temperatures, while not matching observed conditions perfectly (see Figure 4(a)), does provide a much improved estimation of surface temperatures.

5. Conclusion

Data Assimilation potential in improving model predictability has been investigated in this paper. We have shown that by using a physically based surface emission model as the observation operator we have improved estimation of near surface conditions. Near surface soil moisture retrievals using ARPS/LDAS was shown to follow observed situation well. Surface temperature retrieval was shown to be better when we use the assimilation system than if we did not. While the match between observations and assimilated simulations is not perfect, there is nevertheless a good agreement with the discrepancies being attributed to the fact that the in-situ measurements were made at point locations while the assimilated TBs were obtained over areal extents representing the satellite footprint resampled to a 10km spatial resolution.

From the results presented, we showed that in general, soil moisture estimation without assimilation is higher than the corresponding assimilation case. This can be in part due to the uncertainties in modelling microphysics and convection in the adopted mesoscale model. We have demonstrated that by using LDAS, satellite TB observations can be used to improve soil moisture and surface temperature estimations. While both cases depend on initial conditions, poor initial conditions were demonstrated as severely impacting the non assimilation case as the assimilation case is able to recover by assimilating passive microwave TBs. This means that if uncertainties in mesoscale modelling are resolved, then assimilation of lower frequency microwave TBs will yield much more reliable soil moisture estimates.

It has been demonstrated that by improving the land surface conditions, the surface precipitation rates also improve which if therefore used to feed the atmosphere component of a mesoscale model will in turn yield improved estimation of the atmosphere conditions. In such a

*Corresponding author (David Kuria). Tel: +254-727-399208. E-mail addresses: dn.kuria@gmail.com.

scheme, the modified Kain-Fritsch convection scheme can address convection while a microphysics scheme such as the Schultz scheme (Schultz, 1995) addressing the five main hydrometeor categories can be used.

Other satellite platforms operating at microwave frequencies such as the Tropical Rainfall Monitoring Mission and the future Global Precipitation Mission, together with AMSR-E can provide periodic passive microwave data (brightness temperatures) which can be used in the LDAS presents, to improve estimation and forecasting the evolution of surface conditions (soil moisture, surface temperature among others).

6. Acknowledgement

This study was carried out as part of the CEOP and Verification Experiment for AMSR/AMSR-E. Model validation data were provided by the CEOP University of Tokyo Data Archiving Manager Mr. Katsunori Tamagawa. Dr. Kenji Taniguchi provided in-situ dataset. The authors would like to thank them for their support towards this research effort. A very special thank you is due to Associate Professor Dr. Mirza Raza and Dr. Mohammed Rasmy for insightful comments, helping clarify and improve the manuscript.

7. References

Bannister, R.N., (2001). *Elementary 4D-VAR*. Technical report, DARC, University of Reading.

Boussetta, S., (2005). Development of a Land-Atmosphere Coupled Data Assimilation System for physical downscaling. PhD thesis, University of Tokyo.

Choudhury, B.J., Schmugge, T.J., Chang, A. and Newton, R.W., (1979). Effect of surface roughness on the microwave emission from soil. *Geophysical Research*, 84, 5699–5706.

Daley, R., 1991, *Atmospheric Data Analysis*. Cambridge University Press.

Fujii, H. and Koike, T., (2001). Development of a TRMM/TMI algorithm for precipitation in the Tibetan Plateau by considering effects of land surface emissivity. *Journal of the Meteorological Society of Japan*, 79, 475–483.

Huffman, G.J., Adler, R., Morrissey, M., Curtis, S., Joyce, R., McGavock, B. and Susskind, J., (2001). Global precipitation at one-degree daily resolution from multi-satellite observations. *Journal of Hydrometeorology*, 2, 36–50.

Ide, K., Courtier, P., Gill, M. and Lorenc, A.C., (1997). Unified Notation for Data Assimilation: Operational, Sequential and Variational. *Journal of the Meteorological Society of*

Japan, 1–20.

Ingber, L., (1993). Simulated annealing: Practice versus theory. *Mathematical and Computer Modelling*, 18, 29–57.

Kain, J.S. and Fritsch, J.M., (1993). Convective parameterization for mesoscale models: The Kain-Fritsch scheme, the representation of cumulus convection in Numerical Models, Meteorology Monogram . American Meteorology Society.

Kirkpatrick, S.C., Jr., C.D.G. and Vecchi, M.P., (1983). Optimization by Simulated Annealing. *Science*, 220, 671–680.

Kuria, D., Koike, T., Lu, H., Tsutsui, H. and Graf, T., 2007, Field-supported verification and improvement of a passive microwave surface emission model for rough, bare and wet soil surfaces by incorporating shadowing effects. *IEEE Transactions on Geoscience and Remote Sensing*, 45, 1207–1216.

Lin, Y.L., Farley, R.D. and Orville, H.D., (1983). Bulk parameterization of the snow field in a cloud model. *Journal of Climate and Applied Meteorology*, 22, 1065–1089.

Mahadevan, P., Koike, T., Fujii, H., Tamagawa, K., Li, X. and Kaihotsu, I., (2007). Modification and application of the satellite based Land Data Assimilation Scheme for very dry soil regions using AMSR-E images: Model validation for Mongolia — a CEOP data platform. *Journal of the Meteorological Society of Japan*, 85A, 243–260.

Mahadevan, P., Koike, T. and Li, X., 2003, A New Satellite-Based Data Assimilation Algorithm to Determine Spatial and Temporal Variations of Soil Moisture and Temperature Profiles. *Journal of the Meteorological Society of Japan*, 81, 1111–1135.

Njoku, E.G., (1999). AMSR Land surface parameters: Algorithm theoretical basis document, NASA JPL.

Paloscia, S. and Pampaloni, P., (1988). Microwave Polarization Index for Monitoring Vegetation Growth. *IEEE Transactions on Geoscience and Remote Sensing*, 26, 617–621.

Reichle, R.H., Entekhabi, D. and McLaughlin, D.B., (2001). Downscaling of radio brightness measurements for soil moisture estimation: A four-dimensional variational data assimilation approach. *Water Resources Research*, 37, 2353–2364.

Sellers, P.J., Los, S.O., Tucker, C.J., Justice, C.O., Dazlich, D.A., Collatz, G.J. and Randall, D.A., 1996, A revised land surface parameterization (SiB2) for atmospheric GCMs, Part II: the generation of global fields of terrestrial biophysical parameters from satellite data. *Journal of Climate*, 9, 706–737.

Sellers, P.J., Sud, Y.C. and Dalcher, A., 1986, A simple biosphere model (SiB) for use within General Circulation Models. *Journal of the Atmospheric Sciences*, 43, 505–531.

Schultz, P., 1995. An explicit cloud physics parameterization for operational numerical weather prediction. *Monthly Weather Review*, 123, 3331 – 3343.

*Corresponding author (David Kuria). Tel: +254-727-399208. E-mail addresses: dn.kuria@gmail.com.

Tsang, L., Kong, J.A.U. and Shin, R.T., 1985, *Theory of Microwave remote sensing*. Wiley and Sons, New York.

Truong, N. M., Tien, T. T., Pielke Sr., R. A., Castro, C. L. and Leoncini, G., (2009). A modified Kain-Fritsch scheme and its application for the simulation of an extreme precipitation event in Vietnam. *Monthly Weather Review*, 137, 766 – 789.

Ulaby, F.T., Moore, R.K. and Fung, A.K., (1981). *Microwave remote sensing: Fundamentals and radiometry*, Vol. 1. Artech House, Norwood, MA.

Wilheit, T., Kummerow, C. and Ferraro, R., (1999). *EOS/AMSR Rainfall*. Algorithm theoretical basis document.

Wilks, D.S., (1999). Multisite downscaling of daily precipitation with a stochastic weather generator. *Climate Research*, 11, 125–136.

Xue, M., Wang, D., Gao, J., Brewster, K. and Droegemeier, K.K., (2003). The Advanced Regional Prediction System (ARPS), storm-scale numerical weather prediction and data assimilation. *Meteorology and Atmospheric Physics*, 82, 139–170.

Yang, K., Chen, Y.Y. and Qin, J., (2009). Some practical notes on the land surface modeling in the Tibetan Plateau. *Hydrology and Earth System Sciences Discussions*, 6, 1291–1320.

David Kuria is a Senior Lecturer in the department of Geomatic Engineering and Geospatial Information Science of the Kimathi University College of Technology. He received his B. Sc (Surveying) with Honors from the University of Nairobi (Kenya) in 1998. He holds an M. Sc (Photogrammetry and Geoinformatics) from the Stuttgart University of Applied Sciences (Germany) awarded in 2003. He undertook Ph.D. studies at the University of Tokyo (Japan) completing it in 2007. He has lectured for more than 4 year at the Jomo Kenyatta University of Agriculture and Technology. Dr. Kuria's current interests are in webmapping, climate research and geospatial application development.

Toshio Koike received the B.Eng., M.Eng., and D.Eng. degrees from the University of Tokyo, Tokyo, Japan, in 1980, 1982, and 1985, respectively. He was a Research Associate at the University of Tokyo in 1985 and was appointed as an Assistant Professor at the same university in 1986. He was also appointed as an Associate Professor at Nagaoka University of Technology, Nagaoka, Japan in 1992. He has been a Professor at the River and Environmental Engineering Laboratory, Department of Civil Engineering, University of Tokyo since 2000. He is the Lead Scientist of the Coordinated Enhanced Observing Period project. Prof. Koike's research interests are in hydrology, water resources, satellite remote sensing, climate change, and Asian monsoons.

Souhail Boussetta received B.Eng, and M.Eng degrees from the National school of Engineering of Tunis at the University of Tunis in 1991 and 1993 respectively, and a Ph.D from the University of Tokyo, Japan in 2005. He was a Research Associate at the University of Tokyo in 2006 and was appointed as Assistant Professor for EDITORIA at the University of Tokyo in 2007. He is currently a scientist at the European Centre for Medium range Weather Forecast. Dr. Boussetta's research interests include Land surface parameterization, land data assimilation, and satellite remote sensing applied to water resources.

Peer Review: This article has been internationally peer-reviewed and accepted for publication according to the guidelines given at the journal's website.